Journal Pre-proofs

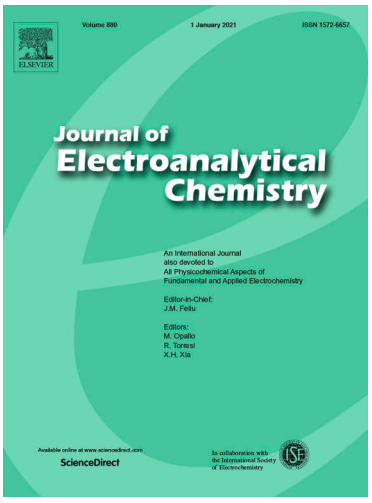

Theoretical insights into homogeneous catalysis impact on ion transfer-electron transfer coupled processes at thick-film modified electrodes

R.A. Fernández, F.M. Zanotto, S.A. Dassie

PII: S1572-6657(24)00434-X
DOI: https://doi.org/10.1016/j.jelechem.2024.118456
Reference: JEAC 118456

To appear in: *Journal of Electroanalytical Chemistry*

Received Date: 30 April 2024
Revised Date: 11 June 2024
Accepted Date: 19 June 2024

Please cite this article as: R.A. Fernández, F.M. Zanotto, S.A. Dassie, Theoretical insights into homogeneous catalysis impact on ion transfer-electron transfer coupled processes at thick-film modified electrodes, *Journal of Electroanalytical Chemistry* (2024), doi: https://doi.org/10.1016/j.jelechem.2024.118456

Theoretical insights into homogeneous catalysis impact on ion transfer-electron transfer coupled processes at thick-film modified electrodes.

R.A. Fernández[1,2,*], F.M. Zanotto[1,2,3,4], S.A. Dassie[1,2]

[1] Universidad Nacional de Córdoba. Facultad de Ciencias Químicas. Departamento de Fisicoquímica. Ciudad Universitaria. X5000HUA. Córdoba. Argentina.

[2] Instituto de Investigaciones en Fisicoquímica de Córdoba (INFIQC), CONICET. Ciudad Universitaria. X5000HUA. Córdoba. Argentina.

[3] Current address: Laboratoire de Réactivité et Chimie des Solides (LRCS), Université de Picardie Jules Verne, Hub de l'Energie, UMR CNRS 7314, 15 rue Baudelocque, 80039 Amiens Cedex 1, France

[4] Current address: Réseau sur le Stockage Electrochimique de l'Energie (RS2E), Hub de l'Energie, FR CNRS 3459, 15 rue Baudelocque, 80039 Amiens Cedex 1, France

[*]**Corresponding author:** ***e-mail address*****:** afernandez@unc.edu.ar

Abstract:

The ion transfer-electron transfer coupled reactions that occur in thick-film modified electrodes is analysed in this work, including a homogeneous catalytic reaction in one of the phases. The model of two polarized interfaces composed in series presented investigates the similarities and differences that arise when compared with the classical electrochemical chemical catalytic mechanism (EC') in a single electrode|solution interface. Special attention is paid to the charge balance of the diffusive flux at each of these two interfaces and to the distribution of the total applied potential at each one. The aim is to find how the applied potential is distributed between the S|L interface and the L|L interface and its dependence on simple external parameters. This will allow us to fully understand the system for its future application in the interfacial electrosynthesis of new materials.

Keywords: ion transfer-electron transfer coupled reactions; thick-film modified electrodes; homogeneous redox catalysis, diffusion-controlled current.

1. Introduction

Nearly half a century ago, Prof. Savéant and co-workers introduced the concept of homogeneous redox catalysis [1–6]. This is an alternative Electrochemical-Chemical mechanism with a catalytic reaction (EC´) where a redox catalyst couple (Red/Ox^{+}) can react

on the electrode surface and then, a homogeneous charge transfer process occurs with a substrate (A) in solution [7–14]. The electrode can continuously serve as a source or a sink of electrons while the catalyst couple acts as a mediator which interacts with a substrate to yield a product of interest through a homogeneous charge transfer. The process also regenerates one of the species of the redox catalyst couple. Generally, the mediator, also called redox shuttle [15], is used to achieve a more efficient electron transfer between the electrode and the substrate. Therefore, low overpotential is required for this indirect process to take place. A practical example of this is the homogeneous oxidation of aliphatic amines in aprotic media by electrochemically generated ferrocenium, which acts as a suitable mediator [16].

In addition, one existing strategy for the study of solid|liquid (S|L) and liquid|liquid (L|L) interfaces simultaneously, is the use of both of them in series in an electrochemical system. This can be accomplished e.g. by covering an electrode with a thick film of organic electrolyte and submerging it in an aqueous immiscible electrolyte. In this setup, two polarized interfaces are created. Thus, electrochemical processes involve the simultaneous injection-ejection of ions through a L|L interface with coupled electron transfer reaction at a S|L interface. At the same time, the total applied potential on the system is distributed between these two interfaces, according to the concentration ratios of the involved species at each one of them [17,18][19]. Similar approaches combining coupled ion transfer-ion transfer were previously described for supported liquid membranes [20][21][22][23].

In recent years, we have worked in different theoretical studies on the thick film modified electrode strategy [19,24]. A general model of a thick organic film-modified electrode has been proposed to analyse the facilitated proton transfer-electron transfer coupled reactions (FPT-ET reactions) in presence of aqueous buffer solutions [24,25]. Furthermore, analytical equations to calculate the half-wave potential for the FPT-ET reactions at thick organic film-modified electrodes (including ion pairing in the organic phase and considering a non-ideal electrolyte solution in both phases) have also been developed [25]. Theoretical and experimental approaches were integrated for the study of these systems, considering some analytical applications derived from fundamental electrochemical features [25,26]. Finally, water autoprotolysis-electron transfer coupled reactions was explored, obtaining detailed mechanistic information at thick-film modified electrodes [27]. In these previously published works, emphasis was placed on different ion transfer processes that occur at the L|L interface (i.e.: simple ion transfer, facilitated proton transfer and facilitated proton transfer via water hydrolysis). Now the effect of homogeneous chemical reactions coupled to the electron transfer process at the S|L interface is explored.

In this work, we contribute to the insight into these systems with a model that considers two polarized interfaces arranged in series (S|L|L interfaces), including a homogeneous catalytic reaction in one of the phases. The ion transfer-electron transfer coupled reaction is analysed, underlining the similarities and differences that emerge when considering a system composed by S|L|L interfaces or a single one (S|L interface). The flux equality at each of these two interfaces and the distribution of the external potential difference applied between the S|L and L|L interfaces are particularly taken into account.

2. Materials and Methods

2.1 Model

A model considering simultaneous electron transfer at a S|L interface and ion transfer at a L|L interface and including a homogeneous catalytic reaction was developed. A catalyst or

mediator is present in the organic phase, initially as a reduced species (Red). A redox couple species, initially as a reduced species (A) and non-electroactive in the potential range considered, reacts in contact with the catalyst oxidized species (Ox^+) to regenerate the same reduced species (Red) and the redox couple oxidized species (B) (see Scheme 1). Supporting electrolyte is also explicitly considered in the organic phase (OY) and in the aqueous phase (MX). The existing interfacial equilibria are the following:

$$\mathrm{Red\,(o)} \rightleftharpoons \mathrm{Ox^+(o)} + e^- \qquad \text{(R.1)}$$

$$\mathrm{Anion^-(o)} \rightleftharpoons \mathrm{Anion^-(w)} \qquad \text{(R.2)}$$

$$\mathrm{Cation^+(w)} \rightleftharpoons \mathrm{Cation^+(o)} \qquad \text{(R.3)}$$

where $\mathrm{Cation^+} \equiv \mathrm{M^+;O^+}$ and $\mathrm{Anion^-} \equiv \mathrm{X^-;Y^-}$

while the homogeneous catalytic reaction is:

$$\mathrm{Ox^+(o) + A\,(o)} \underset{k_b}{\overset{k_f}{\rightleftharpoons}} \mathrm{Red(o) + B(o)} \qquad \text{(R.4)}$$

where $k_f\left(\mathrm{M^{-1}s^{-1}}\right)$ and $k_b\left(\mathrm{M^{-1}s^{-1}}\right)$ are the forward and backward rate constants. The general case involves a second-order reaction.

In order to deduce the model for ion transfer-electron transfer coupled reactions, the same set of assumptions as those in a previous paper were made [19]. These correspond to the points (1)-(11) mentioned in Ref. [19]. Assumptions (12)-(14) are included in this work to allow the consideration of homogeneous catalytic reaction:

1. The interfaces between the aqueous and the organic phase and between the electrode and organic phase are stationary and planar.

2. Both phases remain quiescent and contain enough inert electrolyte so that mass transport takes place only by diffusion. The potential drop due to solution resistance is neglected, as well as other common electrochemical phenomena such as adsorption and desorption, double layer charge and discharge.

3. The transfer of the hydrophilic ions H^+ and OH^- is considered negligible in the potential window used in all the experiments shown.

4. The partition of the mediator species to the aqueous phase, either electrically charged (Ox^+) or neutral (Red), is neglected.

5. The redox reaction taking place at the electrode surface and the transfer of the other ions through the L|L interface, are reversible and diffusion controlled, dependent on the Nernst equation.

6. The thickness of the organic phase (L) must be large enough to avoid overlap between the diffusion layers of the species generated or consumed at the S|L interface and the L|L interface, as long as the resistance of the electrolytic solution is minimized.

7. Both interfaces present the same surface area, large enough for edge effects to be negligible. Therefore, the semi-infinite linear condition is assumed.

8. Since the electron transfer and ion transfer processes are coupled, the current at both interfaces must be equal.

9. The activity coefficients for all species are assumed to be equal to one.

10. Neither double-layer effects, adsorption, nor ion-pair formation are considered in the model.

11. The applied potential is distributed between the S|L interface and the L|L interface at any time. The potential difference on the former defines the concentration ratio of the redox species and on the latter the ion concentration ratios.

12. For simplicity, the partition of the A and B species to the aqueous phase, either electrically charged or neutral, is neglected.

13. The presence of the aqueous phase does not affect the kinetics of the homogeneous catalytic reaction in the organic phase.

14. A and B are non-electroactive species on the electrode surface at the potential range considered.

These assumptions allow for the simulation of current-potential responses by numerically solving Fick's equations of diffusion for all species in one spatial dimension. The explicit finite difference method was used for this work [24,26–31]. The S|L interface is defined to be at $x = 0$ and the L|L interface at $x = L$, as shown in Scheme 1. The value of L was set as $12\sqrt{D_{\max} t_{\max,\exp}}$, where $D_{\max}$ is the highest of the diffusion coefficients and $t_{\max,\exp}$ is the maximum duration between all of the simulations, this guarantees that diffusion layers do not overlap (assumption 6) [19,24–27]. The organic phase contains the catalyst or mediator (Red and Ox^+), a redox couple (A and B), and both phases can contain all of the remaining species (M^+, X^-, O^+ and Y^-). The Red and A species are initially dissolved in the organic phase (in respective concentrations $c_{\mathrm{Red}}^{\mathrm{init}}$ and $c_{\mathrm{A}}^{\mathrm{init}}$). The organic (OY) and the aqueous (MX) supporting electrolytes are initially dissolved in their respective phases (in respective concentrations $c_{\mathrm{OY}}^{\mathrm{init}}$ and $c_{\mathrm{MX}}^{\mathrm{init}}$). All of the electrolytes are considered to be completely dissociated. In order to start simulations at equilibrium, the distribution potential ($\Delta_{\mathrm{o}}^{\mathrm{w}}\phi_{\mathrm{eq}}$) was calculated from the analytical concentrations and the standard transfer potential for each ion i ($\Delta_{\mathrm{o}}^{\mathrm{w}}\phi_i^{\mathrm{o}}$) by adapting the approach developed in Ref. [24,25,32]. All equilibrium concentrations can be calculated from this distribution potential. The initial potential difference (at $t = 0$) is calculated as the sum of the Galvani potential difference at each interface: $E(0) = \Delta_{\mathrm{o}}^{\mathrm{s}}\phi(0) + \left[-\Delta_{\mathrm{o}}^{\mathrm{w}}\phi(0)\right]$ [19,24,26,27,33]. The Galvani potential difference between the electrode and the organic phase is calculated from the initial concentrations of the Red and Ox^+ species which are externally

fixed, while $\Delta_o^w\phi(0)$ is set equal to the distribution potential at the L|L interface, calculated as described above [19,24,25,27,33].

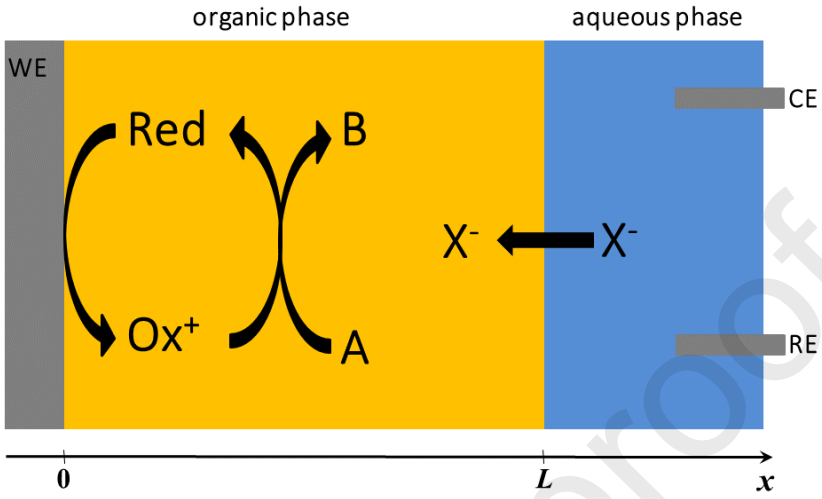

Scheme 1: Schematic representation of reactions involving electron transfer at the S|L interface and ion transfer at the L|L interface. Homogeneous catalytic reaction (R.4) is schematized. WE: working electrode, RE: reference electrode, CE: counter electrode.

The boundary conditions involve the Nernst equation for the coupled processes, i.e. electron transfer and the transfer of ion *i*:

$$\frac{c_{Ox^+}(0,t)}{c_{Red}(0,t)}\left[\frac{c_i^w(L,t)}{c_i^o(L,t)}\right]=\exp\left\{\frac{F}{RT}\left[E(t)-\Delta_o^s\phi_{Red}^o+\Delta_o^w\phi_i^o\right]\right\} \quad (1)$$

where $c_{Ox^+}(0,t)$ and $c_{Red}(0,t)$ are the mediator species concentrations at $x=0$ (S|L interface) at time *t*, $c_i^w(L,t)$ and $c_i^o(L,t)$ are the concentrations of ion *i* at $x=L$ (L|L interface) at time t, $E(t)$ is the externally applied potential, $\Delta_o^s\phi_{Red}^o$ is the standard reduction potential associated to Reaction R.1. and $\Delta_o^w\phi_i^o$ is the standard transfer potential of ion *i*. This condition, together with assumption 11, which can be mathematically expressed as:

$$E(t)=\Delta_o^s\phi(t)+\left[-\Delta_o^w\phi(t)\right] \quad (2)$$

where $\Delta_o^s\phi(t)$ and $\Delta_o^w\phi(t)$ are the Galvani potential differences across the S|L and L|L interfaces at time *t*, respectively, implies that the electron transfer at the S|L interface satisfies its Nernst equation, as well as each ion at the L|L interface [19,33]. Considering the effect of the homogeneous catalytic reaction (R.4) to be negligible, the ratio $\frac{c_{Ox^+}(x,0)}{c_{Red}(x,0)}$ was fixed for all

cases as 10^{-6}, since for values lower than 10^{-4}, no significant changes were observed. This allows for the determination of the initial S|L potential difference, and the initial external potential difference, $E(0)$, from Eqs. (1) and (2).

Additional boundary conditions include the flux equality at $x = 0$ for the mediator species,

$$D^{o}_{Ox^+} \frac{\partial c_{Ox^+}(0,t)}{\partial x} = -D^{o}_{Red} \frac{\partial c_{Red}(0,t)}{\partial x} \tag{3}$$

for the redox couple (assumption 14),

$$\frac{\partial c_A(0,t)}{\partial x} = \frac{\partial c_B(0,t)}{\partial x} = 0 \tag{4}$$

and flux equality at $x = L$ for every ionic species:

$$D^{o}_{i} \frac{\partial c^{o}_{i}(L,t)}{\partial x} = D^{w}_{i} \frac{\partial c^{w}_{i}(L,t)}{\partial x} \tag{5}$$

where *i* represents each of the ions.

Assumption (8) requires the current at both interfaces to be equal. This can be expressed mathematically as:

$$\sum_i z_i D^{w}_{i} \frac{\partial c^{w}_{i}(L,t)}{\partial x} = D^{o}_{Ox^+} \frac{\partial c_{Ox^+}(0,t)}{\partial x} \tag{6}$$

Finally, semi-infinite diffusion conditions imply:

$$c_{Ox^+}(L,t) = c_{Ox^+}(x,0) \tag{7}$$

$$c_{Red}(L,t) = c^{init}_{Red} \tag{8}$$

$$c_A(L,t) = c^{init}_{A} \tag{9}$$

$$c_B(L,t) = c_B(x,0) \tag{10}$$

$$c^{o}_{i}(0,t) = c^{o}_{i}(x,0) \tag{11}$$

$$c^{w}_{i}(\infty,t) = c^{w}_{i}(x,0) \tag{12}$$

for any species *i* except Ox^+, Red, A and B, where the superindex init denotes initial values for the variable.

In this work, cyclic voltammograms are simulated by applying the following external potential:

$$E(t)=\begin{cases}\Delta_{o}^{s}\phi(0)-\Delta_{o}^{w}\phi(0)-vt & \text{if } t\le\lambda\\ \Delta_{o}^{s}\phi(0)-\Delta_{o}^{w}\phi(0)+v(t-2\lambda) & \text{if } t>\lambda\end{cases} \tag{13}$$

where v is the potential sweep rate.

In the potential region where the homogeneous catalytic reaction occurs, the diffusion mass transport for all species of interest follows the relationships:

$$\frac{\partial c_{\mathrm{Red}}^{o}(x,t)}{\partial t}=D_{\mathrm{Red}}^{o}\frac{\partial^2 c_{\mathrm{Red}}^{o}(x,t)}{\partial x^2}+k_f c_{\mathrm{Ox^+}}^{o}(x,t)c_{\mathrm{A}}^{o}(x,t)-k_b c_{\mathrm{Red}}^{o}(x,t)c_{\mathrm{B}}^{o}(x,t)$$

$$\frac{\partial c_{\mathrm{Ox^+}}^{o}(x,t)}{\partial t}=D_{\mathrm{Ox^+}}^{o}\frac{\partial^2 c_{\mathrm{Ox^+}}^{o}(x,t)}{\partial x^2}-k_f c_{\mathrm{Ox^+}}^{o}(x,t)c_{\mathrm{A}}^{o}(x,t)+k_b c_{\mathrm{Red}}^{o}(x,t)c_{\mathrm{B}}^{o}(x,t)$$

$$\frac{\partial c_{\mathrm{B}}^{o}(x,t)}{\partial t}=D_{\mathrm{B}}^{o}\frac{\partial^2 c_{\mathrm{B}}^{o}(x,t)}{\partial x^2}+k_f c_{\mathrm{Ox^+}}^{o}(x,t)c_{\mathrm{A}}^{o}(x,t)-k_b c_{\mathrm{Red}}^{o}(x,t)c_{\mathrm{B}}^{o}(x,t) \tag{14}$$

$$\frac{\partial c_{\mathrm{A}}^{o}(x,t)}{\partial t}=D_{\mathrm{A}}^{o}\frac{\partial^2 c_{\mathrm{A}}^{o}(x,t)}{\partial x^2}-k_f c_{\mathrm{Ox^+}}^{o}(x,t)c_{\mathrm{A}}^{o}(x,t)+k_b c_{\mathrm{Red}}^{o}(x,t)c_{\mathrm{B}}^{o}(x,t)$$

and,

$$\frac{\partial c_i^{\alpha}(x,t)}{\partial t}=D_i^{\alpha}\frac{\partial^2 c_i^{\alpha}(x,t)}{\partial x^2} \tag{15}$$

where index i indicates ionic species.

A modification of the Powell hybrid method [34–39] was used to solve Eqs. (1)-(15) which describe the boundary conditions for the diffusion differential equations. The time step was chosen in order for the simulation to converge for all tested conditions. Experimental time and space are divided in M ($\delta t = t_{\mathrm{exp}}/M$) and N ($\delta x \le \sqrt{2D_{\mathrm{max}}\delta t}$) subintervals [29]. The number of time steps (M) and the number of boxes (N) used in the simulation depend on the kinetic constants of the homogeneous chemical reaction and on the maximum diffusion coefficient (D_{max}). In order to avoid oscillations in the numerical computation, the value of both $\lambda_f\left(=k_f c_{\mathrm{Red}}^{\mathrm{init}}\right)$ and $\lambda_b\left(=k_b c_{\mathrm{Red}}^{\mathrm{init}}\right)$ have to be lower than 0.1 [29]. According to this, a minimum value of M can be defined as follows [40]:

$$M>\begin{cases}10\lambda_f t_{\mathrm{exp}} \text{ if } \lambda_f \ge \lambda_b\\ 10\lambda_b t_{\mathrm{exp}} \text{ if } \lambda_f < \lambda_b\end{cases} \tag{16}$$

where $t_{\exp} = 2\left(\Delta\phi_{final} - \Delta\phi_{initial}\right)/v$ with $\Delta\phi_{final}$ and $\Delta\phi_{initial}$ being the final and initial potential values. Results were checked for step size independence.

3. Results and discussion

In first section, we analyse the ion transfer-electron transfer coupled reactions in the presence of a homogeneous catalytic reaction. This allows understanding some expected differences of adding a second polarizable interface concerning a conventional homogeneous electrocatalytic system. In the second and third sections, we describe the effect of the ionic concentration in the aqueous phase on the voltammetric response. The outcome at different scan rates and potential cycling of thick-film setup with homogeneous catalytic reaction are also described in these sections.

3.1 Ion transfer-electron transfer coupled reactions in the presence of a homogeneous catalytic reaction.

The thick-film setup offers the unusual versatility that allows working in excess or defect of a redox probe (present in one of the phases) with respect to the ionic species initially dissolved in the other phase. The general behaviour of these conditions has been extensively analysed in previous works, and are used here as initial input [19,24–27]. In the present work, the typical conditions for the thick-film setup, which involve the use of an *excess* of ionic species in the aqueous phase with respect to the redox probe dissolved in the organic phase, is analysed in the first place. In **Fig. 1(a)**, simulated cyclic voltammograms obtained in the presence and in the absence of A species at 0.020 Vs^{-1} are shown.

The initial concentration of redox probe was fixed at one order of magnitude below the initial concentration of the aqueous ionic species. In the presence of 1.00 M concentration of A species, and employing a slow scan rate, a strong loss of reversibility with an enhancement of the anodic peak current is observed. This is a limiting current type profile, similar to a sigmoidal shape, but with a noticeable hysteresis. In these simulations, a useful tool to understand this behaviour is computing the evolution of the concentration profiles of the redox probe as a function of the distance from the S|L interface into the organic phase (**Fig. 1(b)**). As it can be observed, in the presence of A, the profiles of Red and Ox^+ are distinctive, showing a notable decrease in the thickness of the diffusional layer. The corresponding ionic species concentration profiles from the L|L interface as a function of the distance into the aqueous phase are displayed in **Fig. 1(c)**. These profiles show a greater consumption of ionic species into the aqueous phase when A species is present in the organic phase. This is because the catalytic process regenerates Red species, allowing it to continue reacting at the S|L interface, since there remains enough concentration of X^- at the L|L interface [19]. This is also the observed phenomenon in a single interface system. It should be noted that all concentration profiles shown in this work were taken at the switching potential value (E_λ) of the respective cyclic voltammograms. In panels **(d)** and **(e)** of **Fig. 1**, the interfacial concentration profiles at $x = 0$ (S|L interface) and $x = L$ (L|L interface), respectively, can be observed. As the catalytic process occurs, a considerable change in the transfer potential value is observed. Also, a different path of Red and Ox^+ interfacial concentrations is perceived, depending on the direction (forward or backward) of the scan potential values. This is in agreement with the hysteresis observed in the corresponding current-

potential profile in the presence of A species. The presence of A causes a considerable increase of the catalytic current, showing a large consumption of species at the interface with a simultaneous variation of the shape of the current-potential profile.

We analyse the effect of the relationship between the scan rate and the rate of the homogeneous catalytic reaction. As the scan rate increases, the regeneration of Red is kinetically unfavored with respect to the charge transfers. Thus, as it can be observed in **Fig. 2(a),** a peak-shape voltammogram is recovered at the higher calculated scan rate (v=2.000 Vs^{-1}). This behaviour is analogous to that previously described for a conventional electrocatalytic process on a solid electrode, as is depicted in panel (c) of figure 2 in ref [16]. This advises that the depletion of Ox^{+} species next to the S|L interface by the chemical reaction is dependent on the rates of both processes. Likewise, in the thick-film setup, the ionic species at the L|L interface are depleted in *higher* proportion at *lower* scan rates. Consequently, a higher consumption of ionic species is observed at the L|L interface at v = 0.020 Vs^{-1} than at v=2.000 Vs^{-1} (**Fig. 2(b)**), because longer experimental time allows a greater extent of the homogeneous catalytic reaction (R.4). Special attention must be paid to this behaviour because it has significant effect on the value of the potential difference at this interface, as will be analysed in a later section.

Another effect to take into account is that high initial concentrations of A species can significantly reduce the thickness of the layer where the catalysed reaction takes place, bringing it closer to the electrode surface. Analogous concentration profiles at the S|L interface obtained in the presence of A species at E_{λ}, are obtained both at high ($v = 2.000\ \mathrm{V\,s^{-1}}$) and low ($v = 0.020\ \mathrm{V\,s^{-1}}$) scan rates (see **Fig. S1** and **Fig. S2**).

3.2 Effect of the aqueous ionic species concentration on the homogeneous catalytic reaction.

In this section, we focus on monitoring the homogeneous catalytic reaction (Reaction R.4) in the organic phase by controlling the initial concentration ratio between the initial ionic species concentration in the aqueous phase and the initial redox probe concentrations in the organic phase $\left(c_{MX}^{init}/c_{Red}^{init}\right)$. At this point, it is important to clarify that, for simplicity, we describe all the process in terms of the anion concentration of the aqueous electrolyte, but it is clear that all present ions (at aqueous or organic phase) are involved in the process to a greater or lesser extent depending on their values of standard transfer potential across the L|L interface [19,41]. The main insight of this analysis is that since the ionic species does not limit the ion transfer-electron transfer coupled process; the chemical reaction (R.4) can progress inside the organic phase. Two different scenarios, at lower and higher initial concentration of X^{-} with respect to the initial redox probe concentration, can be described by interpreting the voltammetric profiles shown in **Fig. 3(a)**. In great excess of aqueous ionic concentration ($\log\left(c_{MX}^{init}/c_{Red}^{init}\right) \geq 2.00$) a sigmoidal-shaped curve is obtained, because both during the forward and backward scans the oxidation process prevails in these conditions. Nevertheless, if the aqueous ionic species concentrations are not above this concentration threshold, the current-potential profile obtained presents only a forward anodic peak, without the corresponding cathodic signal. In both cases,

Ox^+ species are depleted near the S|L interface by (R.4), but in the latter, X^- is also depleted at the L|L interface during the potential scan.

Because of the electron transfer-ion transfer coupled process, Red species cannot react at the S|L interface if X^- species are not present at the L|L interface. In **Fig. 3(b)** it can be seen that approximately at 0.15V, Red interfacial species at the S|L interface stops reacting, while at the same time, Ox^+ interfacial species stops being produced. Whereas in **Fig. 3(c),** it can be observed that $c^{w}_{X^-}(L,t)$ reaches zero aproximately at 0.15V, thus, if the interfacial X^- concentration at the L|L interface is not in excess with respect to Red interfacial concentration in the S|L interface, the complete process stops. It is worth mentioning here that the addition of a second immiscible phase marks a significant difference with respect to the traditional EC′ mechanism, since although Red and A species are available to react, a limiting current type profile is not reached in the thick film setup. This is exclusively attributed to the concerted ion transfer-electron transfer nature of this process, where the total ion fluxes at the L|L interface must be equal to the charge flux at the S|L interface.

Following with the same setup and the same parameters settings, in **Fig. 4(a)**, voltammograms at increasing scan rates are shown. A progressive increase in the scan rate causes two different effects in each phase, and once again a limiting current type profile is observed. On the aqueous phase, fewer moles of X^- are consumed at the L|L interface at higher scan rates. In the organic phase, as mentioned, the regeneration of Red is kinetically unfavoured. Thus, the interfacial concentration of X^- does not limit the overall electrochemical process. In this instance, it is interesting to analyse how the total applied potential in the system, is distributed between each of the interfaces in series, and its effects. Panels **(b)** and **(c)** of **Fig. 4**, show the external applied potential ($E = \Delta^{s}_{o}\phi + \left[-\Delta^{w}_{o}\phi\right]$) and the individual potential difference for the L|L ($-\Delta^{w}_{o}\phi$) and for the S|L interface ($\Delta^{s}_{o}\phi$) as a function of the experimental time. As it can be observed, at 0.020 Vs^{-1}, for example, $\Delta^{s}_{o}\phi$ remains constant during a large portion of the experimental time (blue line in **Fig. 4(b)**). Almost the opposite behaviour occurs when sweeping at a higher scan rate. At $1.000\ V\ s^{-1}$, the L|L interface acts practically as a non-polarizable interface, that is, its potential difference remains nearly constant in a great range of the experimental time (red line in **Fig. 4(c)**). In this way, we arrive at a noteworthy conclusion: the splitting of the applied external potential between the two serial interfaces can be easily manipulated by varying the scan rate of the voltammetric experiment. The explanation of that is related to the variation in the interfacial concentration of the involved species. In the case of lower scan rates, a great consumption and production of ionic species takes place at the L|L interface, while interfacial species concentration are less variable at the S|L interface during the experiment. The opposite situation occurs at higher scan rates at each one of the interfaces.

The existence of a homogeneous catalytic reaction in the non-aqueous phase ensures the availability of the Red species in the vicinity of the electrode. For a given set of kinetic constants for R.4. and potential scan rates, the total current of the system is controlled by the diffusion of the ionic species and does not depend on the ratio of initial concentrations of the mediator and the redox couple. At low potential scan rate, the Red concentration gradient is high and therefore the current flowing throughout the system (through the S|L interface and the L|L interface) is also high (Eq. (6)). Concomitantly, the ion concentration gradient at the L|L interface is also high, with a high depletion of ionic species on the aqueous side of the L|L interface. In this experimental condition, the availability of ionic species in the aqueous phase conditions the

homogeneous catalytic reaction. If the potential scan rate increases, the voltammogram reaches a limiting current characteristic of a coupled catalytic reaction. At high potential scan rates, a current-potential profile is recovered that responds to a diffusion-controlled and reversible charge transfer process.

3.3 Effect of the successive potential scans on the homogeneous catalytic reaction

Considering the input parameters of the system, it is possible to select the initial conditions to switch between different response patterns during the voltammetric experiment. In **Fig. 5(a)** two consecutive potential scans of simulated cyclic voltammograms are shown. During the first scan, a limiting current type profile is obtained. During the second scan, a higher half-wave potential is observed, and a limiting current is reached until around 0.3 V, where the current begins to drop. This behaviour is related to the depletion of X^- at the L|L interface as shown in panel **(b)** of **Fig. 5**, which corresponds to about 16 s of experimental time at $\nu = 0.200\,\mathrm{V\,s^{-1}}$. At this point of the experiment, a significant change in both interfacial potential differences is observed. Given the interfacial depletion of X^-, the potential difference at the L|L interface undergoes an increase of about 0.15 V (with respect to the applied potential) in a short period, while the S|L interface undergoes a decrease of around 0.2 V in the same time interval. The time at which this split in the potential difference arises can be externally controlled by varying the scan rate.

Therefore, the experimental time at which the depletion of X^- at the L|L interface occurs can be in the first sweep or in subsequent scans. This will depend on the relationship between the scan rate and the kinetic constant of the catalytic reaction. **Fig. 6** shows simulated cyclic voltammograms at the same scan rate for different values of forward rate constants of reaction (R4). As the forward rate constant increases, the current-potential profiles tend to be higher until the depletion of ionic species at the L|L interface.

In the particular set of variables chosen for the simulations in **Fig. 7**, the current drops during the backward scan of the first cycle (see black line) and also drops during the forward scan of the second cycle (see blue line). This gives an approximate idea of the relationship between the two main rate variables that control this process. Whenever this drop in the current value is observed, it signals the experimental time at which the depletion of ionic species at the L|L interface occurs. More strictly, since in a concerted system, the total current must equal to the total ion fluxes at the L|L interface and also to the charge flux at the S|L interface, (see Eq. 5) an insufficient ion flux can be the limiting factor in the total current of the system.

4. Conclusion

As in several previous works [19,24–27] we have studied through simulations the thick-film modified electrode, where the reduction of a redox probe is coupled to the transfer of the most hydrophobic anionic species existent in the aqueous phase, due to the lower global free energy of transfer for this overall process. In this case, we have demonstrated the possibility of using this setup as a convenient system to understand the effect of the ionic concentration in the aqueous phase in the voltammetric response when a catalytic reaction takes place in the organic phase.

In this work it was demonstrated how a set of external parameters such as the potential scan rate, the successive voltammetric cycles and the concentration ratios between the mediator, the redox couple and ionic species allow us to understand how the applied potential is distributed between the S|L interface and the L|L interface.

Given that L|L interfaces offer a reproducible environment for the preparation of interfacial films of interesting materials such as conducting polymers [42,43], certain nanoparticles [44], and their metal composites [45], the experimental setup described in this study will allow the development of promising applications in the interfacial electrosynthesis of thin film materials at the L|L interface.

Recently, coulometric thin layer cell using the conducting polymer-coated electrode have been proposed and used for the realization of stripping voltammetry and absolute determination of redox-inactive ions [46–51]. Clearly, in this experimental setup, ion transfer-electron transfer coupled process occur in a multilayer arrangement of thin films. Although there is a new electrode|electroactive polymer interface and the phases are thin films, the conceptual framework is the same. An extension of the model presented in this work can be used, including at least the resolution of the corresponding Poisson-Boltzmann equation for the calculation of the electric potential at each interface and the Poisson-Nernst-Planck equation for the ion transport [52–54]. The condition of electroneutrality is not obeyed in the systems where the thickness of one of the liquid phases is in the order of magnitude of the Debye screening length [55]. We will include in future research the modelling of systems with thin films such as those used in coulometric thin layer cells.

Acknowledgements

R.A.F. and S.A.D. are researchers from Consejo Nacional de Investigaciones Científicas y Técnicas (CONICET). F.M.Z. thanks CONICET for the fellowship granted. Financial support from CONICET and Secretaría de Ciencia y Tecnología de la Universidad Nacional de Córdoba (SECyT-UNC) are gratefully acknowledged.

References

[1] C.P. Andrieux, J.M. Dumas-Bouchiat, J.M. Saveant, Homogeneous redox catalysis of electrochemical reactions. Part I. Introduction, J. Electroanal. Chem. 87 (1978) 39–53. https://doi.org/10.1016/S0022-0728(78)80378-7.

[2] C.P. Andrieux, J.M. Dumas-Bouchiat, J.M. Saveant, Homogeneous redox catalysis of electrochemical reactions. Part II. Rate determining electron transfer, evaluation of rate and equilibrium parameters, J. Electroanal. Chem. 87 (1978) 55–65. https://doi.org/10.1016/S0022-0728(78)80379-9.

[3] C.P. Andrieux, J.M. Dumas-Bouchiat, J.M. Saveant, Homogeneous redox catalysis of electrochemical reactions. Part III. Rate determining electron transfer. Kinetic characterization of follow-up chemical reactions, J. Electroanal. Chem. 88 (1978) 43–48. https://doi.org/10.1016/S0022-0728(78)80338-6.

[4] C.P. Andrieux, J.M. Dumas-Bouchiat, J.M. Savéant, Homogeneous redox catalysis of electrochemical reactions. Part IV. Kinetic controls in the homogeneous process as characterized by stationary and quasi-stationary electrochemical techniques, J. Electroanal. Chem. 113 (1980) 1–18. https://doi.org/10.1016/S0022-0728(80)80507-9.

[5] C.P. Andrieux, C. Blocman, J.M. Dumas-Bouchiat, F. M'Halla, J.M. Savéant, Homogeneous Redox Catalysis of Electrochemical Reactions. Part V. Cyclic Voltammetry, J. Electroanal. Chem. 113 (1980)

19–40.

[6] J.M. Savéant, K.B. Su, Homogeneous redox catalysis of electrochemical reaction. Part VI. Zone diagram representation of the kinetic regimes, J. Electroanal. Chem. 171 (1984) 341–349. https://doi.org/10.1016/0022-0728(84)80125-4.

[7] R.S. Nicholson, I. Shain, Theory of Stationary Electrode Polarography, Anal. Chem. 36 (1964) 706–723. https://doi.org/10.1021/ac60210a007.

[8] J.M. Savéant, Molecular catalysis of electrochemical reactions. Mechanistic aspects., Chem. Rev. 108 (2008) 2348–2378. https://doi.org/10.1016/j.coelec.2017.02.006.

[9] S.W. Feldberg, J.F. Campbell, The quasicatalytic mechanism: A variation of the catalytic (EC′) mechanism, Anal. Chem. 81 (2009) 8797–8800. https://doi.org/10.1021/ac901309v.

[10] C. Costentin, J.M. Savéant, Homogeneous Catalysis of Electrochemical Reactions: The Steady-State and Nonsteady-State Statuses of Intermediates, ACS Catal. 8 (2018) 5286–5297. https://doi.org/10.1021/acscatal.8b01195.

[11] R.J. Salomi, L. Rajendran, Cyclic voltammetric response of homogeneous catalysis of electrochemical reactions: Part 1. A theoretical and numerical approach for EE'C scheme, J. Electroanal. Chem. 918 (2022) 116429. https://doi.org/10.1016/j.jelechem.2022.116429.

[12] S. Vinolyn Sylvia, L. Rajendran, Cyclic voltammetric response of homogeneous catalysis of electrochemical reactions: Part 2. A theoretical and numerical approach for EC scheme, J. Electroanal. Chem. 918 (2022) 116453. https://doi.org/10.1016/j.jelechem.2022.116453.

[13] B. Manimegalai, L. Rajendran, Cyclic voltammetric response of homogeneous catalysis of electrochemical reaction. Part 3: A theoretical and numerical approach for one-electron two-step reaction scheme, J. Electroanal. Chem. 922 (2022) 116706. https://doi.org/10.1016/j.jelechem.2022.116706.

[14] R.U. Rani, L. Rajendran, M. Abukhaled, Theoretical analysis of homogeneous catalysis of electrochemical reactions: steady-state current–potential, React. Kinet. Mech. Catal. 136 (2023) 1229–1242. https://doi.org/10.1007/s11144-023-02407-x.

[15] M.J. Lacey, J.T. Frith, J.R. Owen, A redox shuttle to facilitate oxygen reduction in the lithium air battery, Electrochem. Commun. 26 (2013) 74–76. https://doi.org/10.1016/j.elecom.2012.10.009.

[16] A.A.J. Torriero, M.J.A. Shiddiky, I. Burgar, A.M. Bond, Homogeneous electron-transfer reaction between electrochemically generated ferrocenium ions and amine-containing compounds, Organometallics. 32 (2013) 5731–5739. https://doi.org/10.1021/om4002318.

[17] M. Zhou, S. Gan, L. Zhong, X. Dong, J. Ulstrup, D. Han, L. Niu, Improvement in the assessment of direct and facilitated ion transfers by electrochemically induced redox transformations of common molecular probes, Phys. Chem. Chem. Phys. 14 (2012) 3659–3668. https://doi.org/10.1039/c2cp23184k.

[18] S. Gan, M. Zhou, J. Zhang, L. Zhong, J. Ulstrup, L. Niu, Ion Transfer Voltammetry Associated with Two Polarizable Interfaces Within Water and Moderately Hydrophobic Ionic Liquid Systems, Electroanalysis. 25 (2013) 857–866. https://doi.org/10.1002/elan.201200123.

[19] F.M. Zanotto, R.A. Fernández, S.A. Dassie, Theoretical model of ion transfer-electron transfer coupled reactions at the thick-film modified electrodes, J. Electroanal. Chem. 784 (2017) 25–32. https://doi.org/10.1016/j.jelechem.2016.11.044.

[20] J. Koryta, Electrochemistry of liquid membranes: Interfacial aspects, Electrochim. Acta. 32 (1987) 419–424. https://doi.org/10.1016/0013-4686(87)85007-7.

[21] Z. Samec, A. Trojánek, J. Langmaier, E. Samcová, Cyclic and convolution potential sweep voltammetry of reversible ion transfer across a liquid membrane, J. Electroanal. Chem. 481 (2000) 1–6. https://doi.org/10.1016/S0022-0728(99)00457-X.

[22] A. Molina, C. Serna, J. Gonzalez, J.A. Ortuño, E. Torralba, Ion transfer across a liquid membrane. General solution for the current-potential response of any voltammetric technique., Phys. Chem. Chem. Phys. 11 (2009) 1159–1166. https://doi.org/10.1039/b816843c.

[23] A. Molina, C. Serna, J.A. Ortuno, E. Torralba, Studies of ion transfer across liquid membranes by electrochemical techniques, Annu. Reports Sect. C Phys. Chem. 108 (2012) 126–176. https://doi.org/10.1039/c2pc90005j.

[24] F.M. Zanotto, R.A. Fernández, S.A. Dassie, Facilitated proton transfer-electron transfer coupled reactions at thick-film modified electrodes, Electrochim. Acta. 258 (2017) 727–734. https://doi.org/10.1016/j.electacta.2017.11.119.

[25] F.M. Zanotto, T.A. Hernández, R.A. Fernández, S.A. Dassie, An integrated theoretical-experimental approach to understand facilitated proton transfer-electron transfer coupled reactions at thick-film modified electrodes, Electrochim. Acta. 283 (2018) 1719–1731. https://doi.org/10.1016/j.electacta.2018.07.053.

[26] F.M. Zanotto, R.A. Fernández, S.A. Dassie, An electroanalytical method for monitoring acid hydrolysis reactions using thick-film modified electrodes, Electrochim. Acta. 380 (2021) 137906. https://doi.org/10.1016/j.electacta.2021.137906.

[27] F.M. Zanotto, R.A. Fernández, S.A. Dassie, Facilitated proton transfer via water autoprotolysis-electron transfer coupled reactions at thick-film modified electrodes, Electrochim. Acta. 349 (2020) 136316. https://doi.org/10.1016/j.electacta.2020.136316.

[28] D.K. Gosser, Cyclic Voltammetry: Simulation and Analysis of Reaction Mechanisms, VCH publishers, New York, 1993.

[29] D. Britz, Digital Simulation in Electrochemistry, 3rd ed., Springer, Berlin Heidelberg, 2005.

[30] A.J. Bard, C.R. Faulkner, Electrochemical Methods, Fundamentals and Applications, Second Ed., John Wiley & Sons, New York, 2001.

[31] J.I. Garcia, R.A. Iglesias, S.A. Dassie, Effect of ligand protonation on the facilitated ion transfer reactions across oil|water interfaces. III. Digital simulation and experimental approach, J. Electroanal. Chem. 586 (2006) 225–236. https://doi.org/10.1016/j.jelechem.2005.10.009.

[32] J.I. Garcia, R.A. Fernández, S.A. Dassie, T. Kakiuchi, Distribution of ionic components between two immiscible solutions. Partition of weak bases, J. Electroanal. Chem. 640 (2010) 42–50. https://doi.org/10.1016/j.jelechem.2009.12.028.

[33] V. Mirčeski, F. Quentel, M. L'Her, A. Pondaven, Studying the kinetics of the ion transfer across the liquid|liquid interface by means of thin film-modified electrodes, Electrochem. Commun. 7 (2005) 1122–1128. https://doi.org/10.1016/j.elecom.2005.08.005.

[34] M.J.D. Powell, A Fortran subroutine for solving systems of nonlinear algebraic equations (free access), Harwell, Berkshire, 1968. https://www.osti.gov/biblio/4772677.

[35] A.M. Ostrowski, Solution of Equations and System of Equations, 2sd Ed, Academic Press Inc, 1966.

[36] M.J.D. Powell, A Hybrid Method for Nonlinear Equations, in: P. Rabinowitz (Ed.), Numer. Methods Nonlinear Algebr. Equations, Gordon and Breach Science Publishers, New York, 1970: pp. 87–114.

[37] M.J.D. Powell, A FORTRAN Subroutine for Solving Systems of Nonlinear Algebraic Equations, in: P. Rabinowitz (Ed.), Numer. Methods Nonlinear Algebr. Equations, Gordon and Breach Science Publishers, New York, 1970: pp. 115–161.

[38] W.H. Press, S.A. Teukolsky, I.T. Vetterling, B.P. Flannery, Numerical Recipes in Fortran 77 The Art of Scientific Computing, 2nd Ed, Cambridge University Press, 1992.

[39] Subroutines in Fortran are free available, (2024). http://www.netlib.org (accessed January 8, 2024).

[40] R.A. Iglesias, S.A. Dassie, A.M. Baruzzi, Optical and voltammetric detection of a coupled chemical reaction after the transfer across a liquid|liquid interface, J. Electroanal. Chem. 556 (2003) 23–33. https://doi.org/10.1016/S0022-0728(03)00325-5.

[41] R.A. Iglesias, S.A. Dassie, Ion Transfer at Liquid|Liquid Interfaces, Nova Publishers, New York, 2010.

[42] R.A. Lehane, A. Gamero-Quijano, S. Malijauskaite, A. Holzinger, M. Conroy, F. Laffir, A. Kumar, U. Bangert, K. McGourty, M.D. Scanlon, Electrosynthesis of Biocompatible Free-Standing PEDOT Thin Films at a Polarized Liquid|Liquid Interface, J. Am. Chem. Soc. 144 (2022) 4853–4862. https://doi.org/10.1021/jacs.1c12373.

[43] A.J.G. Zarbin, Liquid-liquid interfaces: A unique and advantageous environment to prepare and process thin films of complex materials, Mater. Horizons. 8 (2021) 1409–1432. https://doi.org/10.1039/d0mh01676d.

[44] M.D. Scanlon, E. Smirnov, T.J. Stockmann, P. Peljo, Gold Nanofilms at Liquid-Liquid Interfaces: An Emerging Platform for Redox Electrocatalysis, Nanoplasmonic Sensors, and Electrovariable Optics, Chem. Rev. 118 (2018) 3722–3751. https://doi.org/10.1021/acs.chemrev.7b00595.

[45] M.F. Suárez-Herrera, A. Gamero-Quijano, M.D. Scanlon, Electrosynthesis of poly(2,5-dimercapto-1,3,4-thiadiazole) films and their composites with gold nanoparticles at a polarised liquid|liquid interface, Electrochim. Acta. 424 (2022). https://doi.org/10.1016/j.electacta.2022.140677.

[46] Y. Yoshida, S. Yamaguchi, K. Maeda, Conducting polymer-coated electrode as a reference/counter electrode in an organic phase and its application to a two-electrode type thin-layer cell for voltammetry at the liquid | liquid interface, Anal. Sci. 26 (2010) 137–139. https://doi.org/10.2116/analsci.26.137.

[47] E. Grygolowicz-Pawlak, E. Bakker, Thin layer coulometry with ionophore based ion-selective membranes, Anal. Chem. 82 (2010) 4537–4542. https://doi.org/10.1021/ac100524z.

[48] Y. Yoshida, S. Nakamura, J. Uchida, A. Henmi, K. Maeda, A flow electrolysis cell with a thin aqueous phase and a thin organic phase for the absolute determination of trace ionic species, J. Electroanal. Chem. 707 (2013) 95–101. https://doi.org/10.1016/j.jelechem.2013.08.030.

[49] E. Kusakabe, Y. Nakamura, K. Maeda, M. Fukuyama, Y. Yoshida, Effect of oxidation ratio of conducting polymer on potential stability of the conducting polymer-coated electrode in voltammetric cell for the ion transfer, J. Electroanal. Chem. 825 (2018) 8–15. https://doi.org/10.1016/j.jelechem.2018.07.057.

[50] S. Tatsumi, T. Omatsu, K. Maeda, M.P.S. Mousavi, G.M. Whitesides, Y. Yoshida, An all-solid-state thin-layer laminated cell for calibration-free coulometric determination of K+, Electrochim. Acta. 408 (2022) 139946. https://doi.org/10.1016/j.electacta.2022.139946.

[51] R. Iwasaki, J. Uchida, Y. Yamana, Y. Nakamura, K. Maeda, S. Sotoma, Y. Yoshida, Coulometric Determination of Perfluoroalkyl Substances (PFAS) with the Thin-layer Electrolysis Flow Cell for the Ion Transfer, Electrochemistry. 91 (2023) 18–22. https://doi.org/10.5796/electrochemistry.23-00066.

[52] M.Z. Bazant, K.T. Chu, B.J. Bayly, Current-voltage relations for electrochemical thin films, SIAM J. Appl. Math. 65 (2005) 1463–1484. https://doi.org/10.1137/040609938.

[53] D. Yan, M.Z. Bazant, P.M. Biesheuvel, M.C. Pugh, F.P. Dawson, Theory of linear sweep voltammetry with diffuse charge: Unsupported electrolytes, thin films, and leaky membranes, Phys. Rev. E. 95 (2017) 1–20. https://doi.org/10.1103/PhysRevE.95.033303.

[54] M. Rossi, T. Wallmersperger, S. Neukamm, K. Padberg-Gehle, Modeling and Simulation of Electrochemical Cells under Applied Voltage, Electrochim. Acta. 258 (2017) 241–254. https://doi.org/10.1016/j.electacta.2017.10.047.

[55] V.S. Markin, A.G. Volkov, Distribution potential in small liquid-liquid systems, J. Phys. Chem. B. 108 (2004) 13807–13812. https://doi.org/10.1021/jp0485385.

Figure Captions

Figure 1: **(a)** Simulated cyclic voltammograms obtained in absence **(-----)** or in presence **(——)** of 1.00 M initial concentration of **A** species. **(b)** Interfacial concentration profiles of Red species at S|L interface in absence of A species **(-----)** and in presence of A species **(——)** and Ox^+ species in absence of A species **(——)** and in presence of A species **(——)** for the corresponding voltammograms as function of the distance inside the organic phase. Profiles were taken at the switching potential value (E_λ). **(c)** Interfacial concentration profiles at the L|L interface of aqueous X^- species in absence of A species (-----) and in presence of A species (——); and of organic X^- species in absence of A species (——) and in presence of A species (——) for the corresponding voltammograms as function of the distance to the interface. Profiles were taken at the switching potential value (E_λ). **(d)** Interfacial concentration profiles at the S|L interface of Red species in absence of A species **(-----)** and in presence of **A** species **(——)**; and Ox^+ species in absence of A species **(——)** and in presence of A species **(——)** for the corresponding voltammograms as function of the total applied potential difference. **(e)** Interfacial concentration profiles at the L|L interface of aqueous X^- species in absence of A species (-----) and in presence of A species (——); and organic X^- species in absence of A species (——) and in presence of A species (——) for the corresponding voltammograms as function of the total applied potential difference.

Simulation parameters:

$k_f = 25.0\ \mathrm{M^{-1}\,s^{-1}}$, $k_b = 0.0\ \mathrm{M^{-1}\,s^{-1}}$, $\Delta^{\mathrm{w}}_{\mathrm{o}}\phi^{o'}_{\mathrm{X^-}} = -0.100\,\mathrm{V}$, $\Delta^{\mathrm{w}}_{\mathrm{o}}\phi^{o'}_{\mathrm{M^+}} = 0.600\,\mathrm{V}$, $\Delta^{\mathrm{w}}_{\mathrm{o}}\phi^{o'}_{\mathrm{O^+}} = -0.700\,\mathrm{V}$,

$\Delta^{\mathrm{w}}_{\mathrm{o}}\phi^{o'}_{\mathrm{Y^-}} = 0.725\,\mathrm{V}$, $\Delta^{\mathrm{s}}_{\mathrm{o}}\phi^{\mathrm{o}}_{\mathrm{Red}} = -0.050\,\mathrm{V}$, $v = 0.020\ \mathrm{V\,s^{-1}}$, $c^{\mathrm{o}}_{\mathrm{A}} = 1.00\,\mathrm{M}$, $c^{\mathrm{init}}_{\mathrm{Red}} = 5.00\times10^{-4}\ \mathrm{M}$,
$c^{\mathrm{init}}_{\mathrm{MX}} = 5.00\times10^{-4}\ \mathrm{M}$, $c^{\mathrm{init}}_{\mathrm{OY}} = 1.00\times10^{-2}\ \mathrm{M}$, $D^{\mathrm{w}}_{\mathrm{species}} = 1.00\times10^{-5}\ \mathrm{cm^2\,s^{-1}}$ and $D^{\mathrm{o}}_{\mathrm{species}} = \xi^2 D^{\mathrm{w}}_{\mathrm{species}}$ with $\xi = 1.12$ ($\mathrm{H_2O}\,|\,$1,2-DCE interface).

Figure 2: **(a)** Simulated cyclic voltammograms obtained in presence of 1.00M initial concentration of A species at different scan rates. $v = 0.020\ \mathrm{V\,s^{-1}}$ (-----) and $v = 2.000\ \mathrm{V\,s^{-1}}$ (——). **(b)** Interfacial concentration profiles at L|L interface of X^- species in presence of 1.00 M initial concentration of **A** species for the corresponding voltammograms as function of the total applied potential difference, $c^{\mathrm{w}}_{\mathrm{X^-}}(L,t)$ at $0.020\ \mathrm{V\,s^{-1}}$ (——), $c^{\mathrm{o}}_{\mathrm{X^-}}(L,t)$ at $0.020\ \mathrm{V\,s^{-1}}$ (——). $c^{\mathrm{w}}_{\mathrm{X^-}}(L,t)$ at $2.000\ \mathrm{V\,s^{-1}}$ (-----) $c^{\mathrm{o}}_{\mathrm{X^-}}(L,t)$ at $2.000\ \mathrm{V\,s^{-1}}$ (——). $c^{\mathrm{init}}_{\mathrm{MX}} = 5.00\times10^{-2}\ \mathrm{M}$. Other simulation parameters are the same as in **Fig. 1**.

Figure 3: **(a)** Simulated cyclic voltammograms obtained at $v = 0.020\ \mathrm{V\,s^{-1}}$ in presence of 1.00 M initial concentration of **A** species at different X^- initial concentrations: $c^{\mathrm{init}}_{\mathrm{MX}} = 5.00\times10^{-2}\ \mathrm{M}$ **(-----)** and $c^{\mathrm{init}}_{\mathrm{MX}} = 5.00\times10^{-3}\ \mathrm{M}$ **(——)**. **(b)** Interfacial concentration profiles at S|L interface of Red species in presence of 1.00 M initial concentration of **A** species as function of the total applied potential difference. $c^{\mathrm{o}}_{\mathrm{Red}}(0,t)$ **(——)**,

$c^{o}_{Ox^+}(0,t)$ (——). **(c)** Interfacial concentration profiles at L|L interface of X^- species in presence of 1.00 M initial concentration of A species as function of the total applied potential difference. $c^{w}_{X^-}(L,t)$ (——) and $c^{o}_{X^-}(L,t)$ (——). Panels (b) and (c): $c^{init}_{MX} = 5.00\times10^{-3}$ M. Other simulation parameters are the same as in **Fig. 1**.

Figure 4: (a) Simulated cyclic voltammograms obtained in presence of 1.00 M initial concentration of **A** species at different scan rates: $v = 0.020$ V s^{-1} (-----), $v = 0.200$ V s^{-1} (-----) and $v = 1.000$ V s^{-1} (——). **(b)** Potential difference at each interface as a function of the experimental time. External applied potential (-----), individual potential difference for the L|L interface ($-\Delta^{w}_{o}\phi$) (-----) and individual potential difference for the S|L interface ($\Delta^{s}_{o}\phi$) (——). $v = 0.020$ V s^{-1}. **(c)** Potential difference at each interface as a function of the experimental time. External applied potential (-----), individual potential difference for the L|L interface ($-\Delta^{w}_{o}\phi$) (-----), individual potential difference for the S|L interface ($\Delta^{s}_{o}\phi$) (——), $v = 1.000$ V s^{-1}. $c^{init}_{MX} = 5.00\times10^{-3}$ M and oother simulation parameters are the same as in **Fig. 1**.

Figure 5: (a) Simulated cyclic voltammograms obtained in presence of 1.00 M initial concentration of A species at $v = 0.200$ V s^{-1}. First cycle (-----) and second cycle (——). **(b)** Interfacial concentration profiles at L|L interface of X^- species in presence of 1.00 M initial concentration of **A** species as function of the experimental time. $c^{w}_{X^-}(L,t)$ (——) and $c^{o}_{X^-}(L,t)$ (——). **(c)** Potential difference at each interface as a function of the experimental time. Individual potential difference for the L|L interface ($-\Delta^{w}_{o}\phi$) (-----) and individual potential difference for the S|L interface ($\Delta^{s}_{o}\phi$) (——). $c^{init}_{MX} = 5.00\times10^{-3}$ M and other simulation parameters are the same as in **Fig. 1**.

Figure 6: Simulated cyclic voltammograms obtained in presence of 1.00 M initial concentration of A species at $v = 0.200$ V s^{-1}. For different values of forward rate kinetic constant in (R.4) $k_f = 10.00$ M^{-1} s^{-1} (-----), $k_f = 25.00$ M^{-1} s^{-1} (-----), $k_f = 50.00$ M^{-1} s^{-1} (——) and $k_f = 100.0$ M^{-1} s^{-1} (——). Other simulation parameters are the same as in **Fig. 1**.

Figure 7: Simulated cyclic voltammograms obtained in presence of 1.00 M initial concentration of A species at v = 0.150 Vs^{-1}. First cycle (-----) and second cycle (——). Other simulation parameters are the same as in **Fig. 1**.

Figure 1

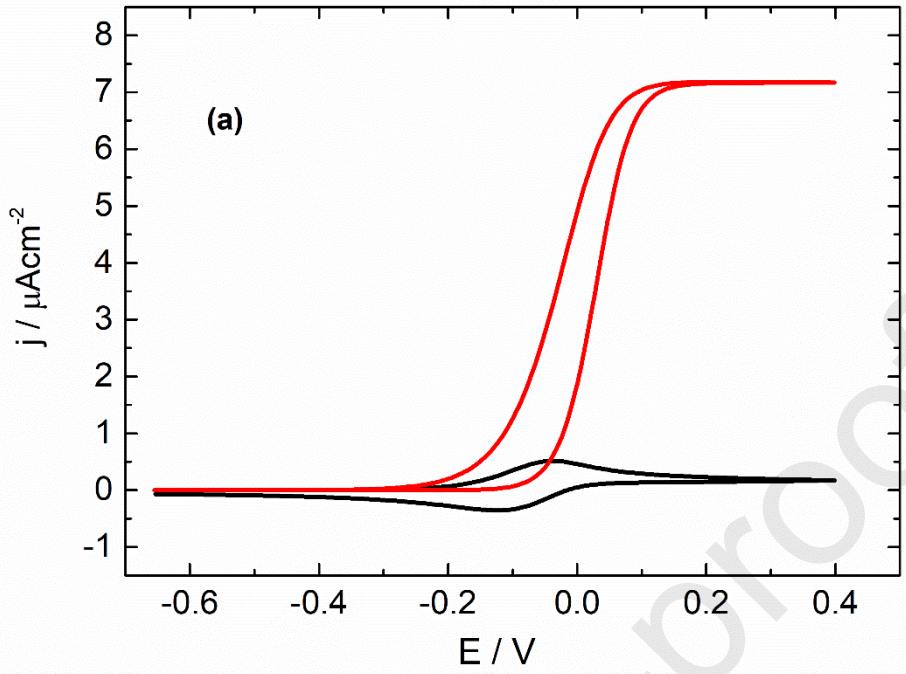

Figure 1

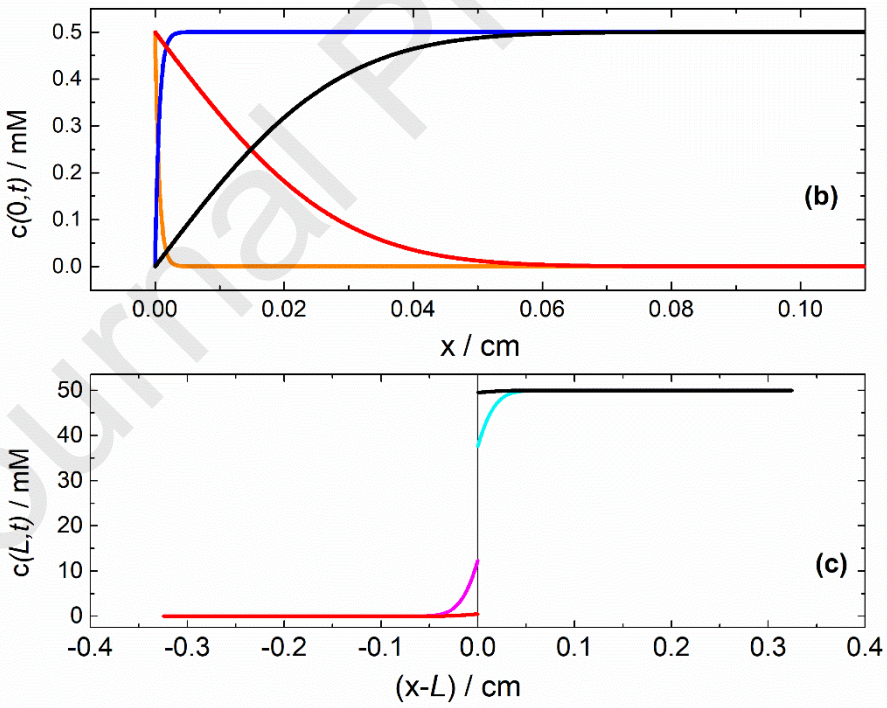

Figure 1

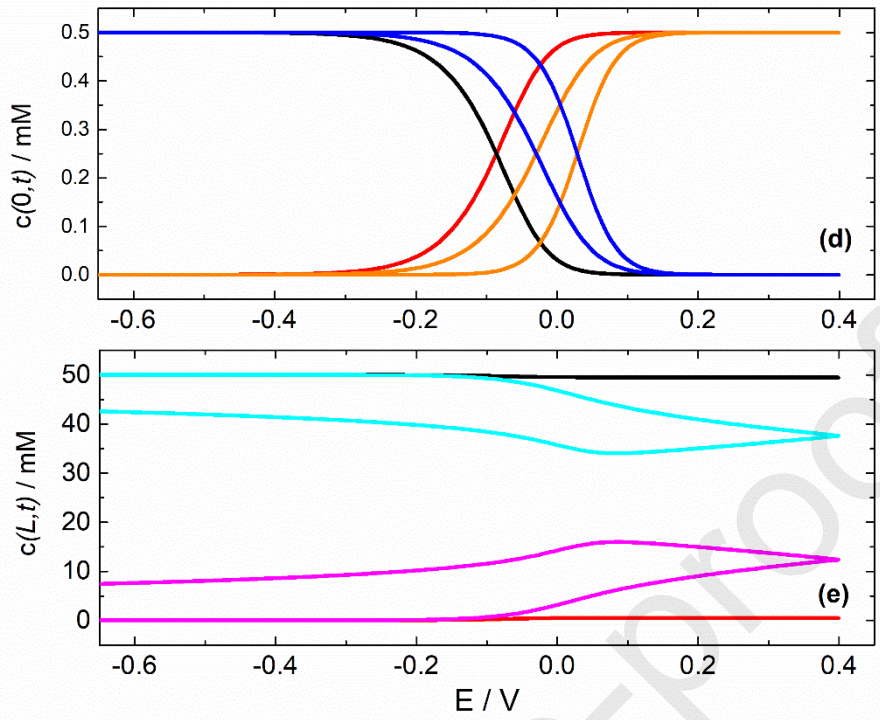

Figure 2

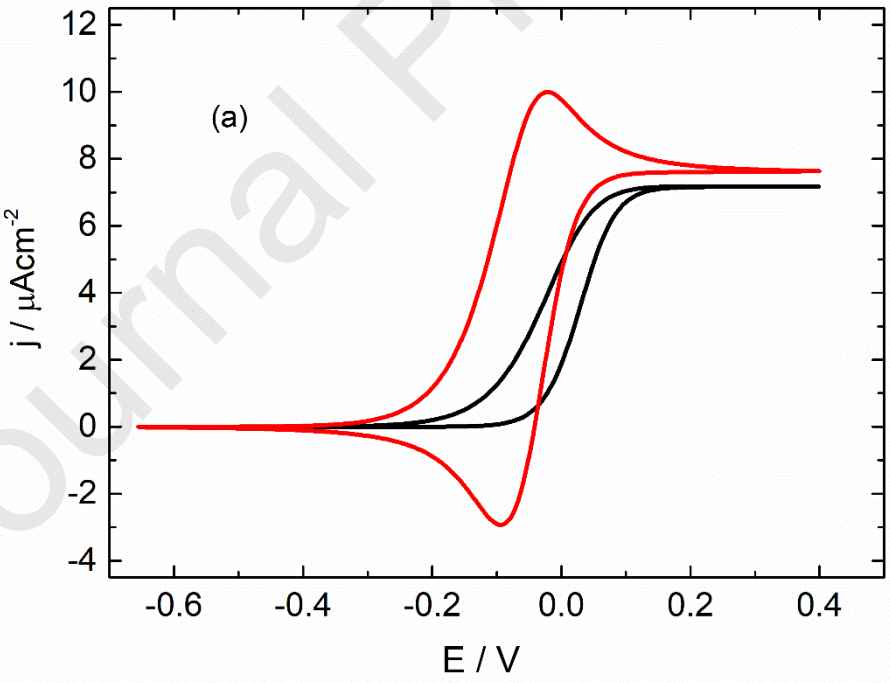

Figure 2.

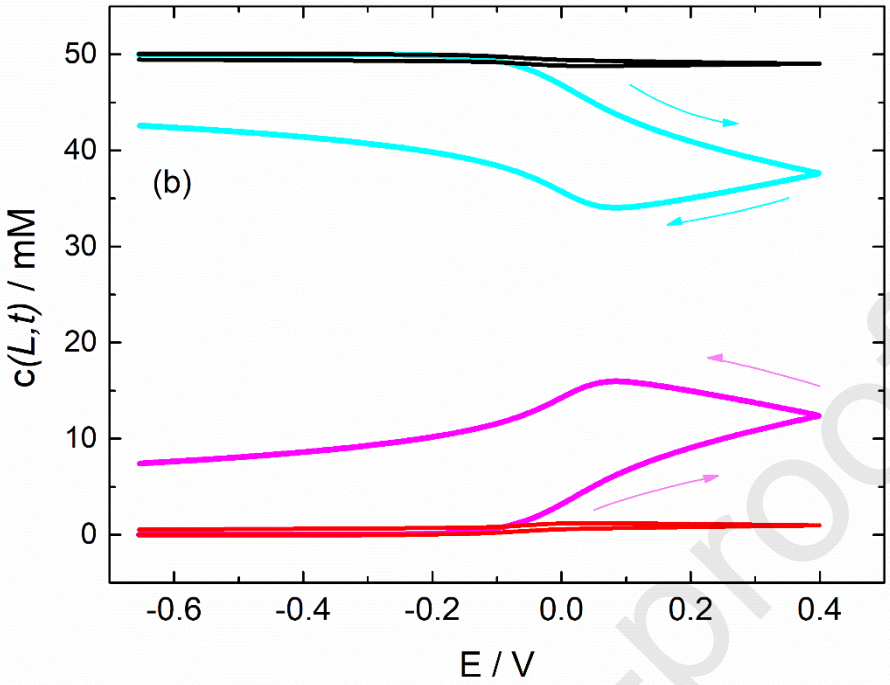

Figure 3

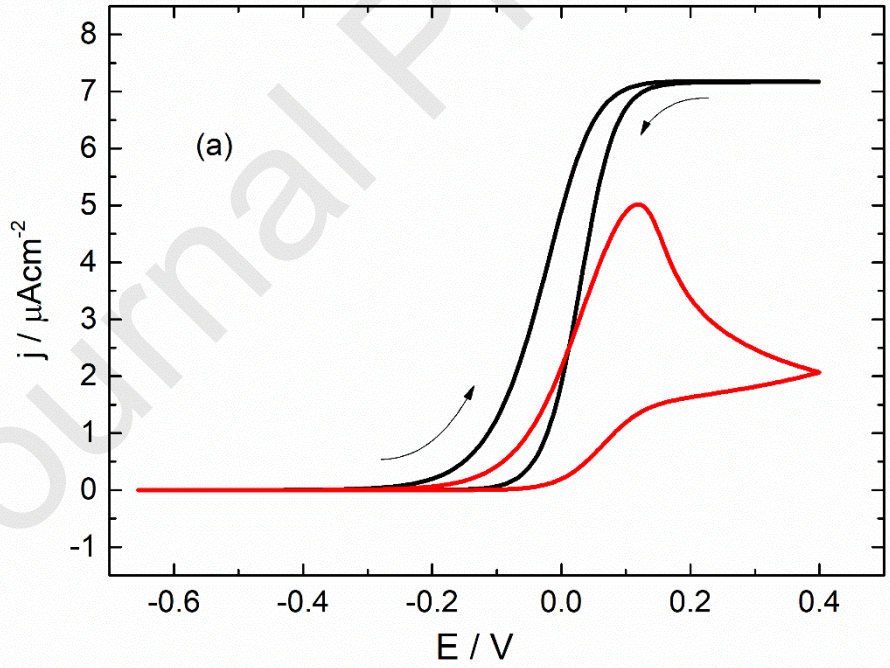

Figure 3

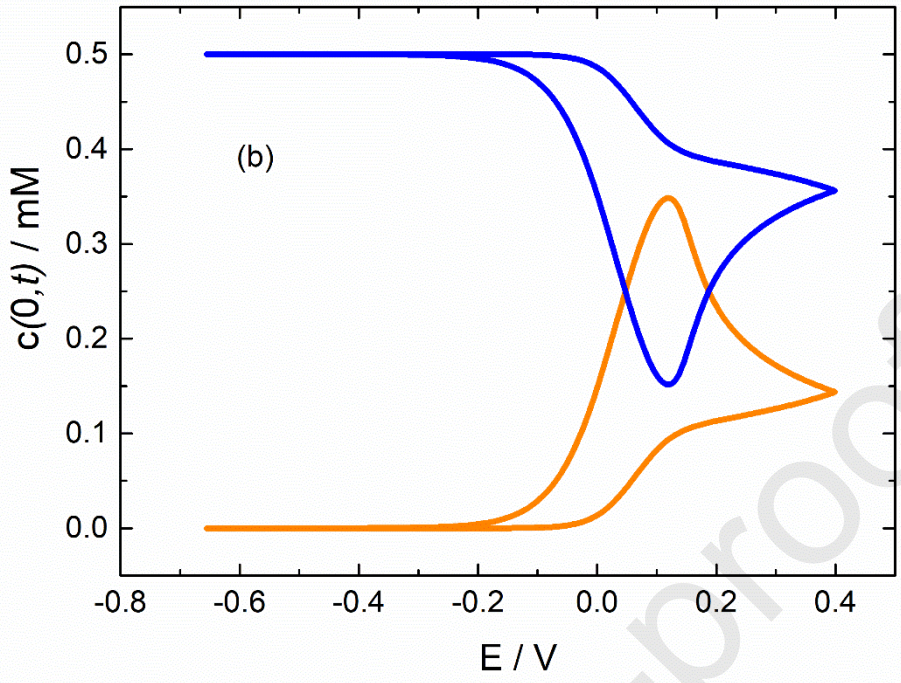

Figure 3

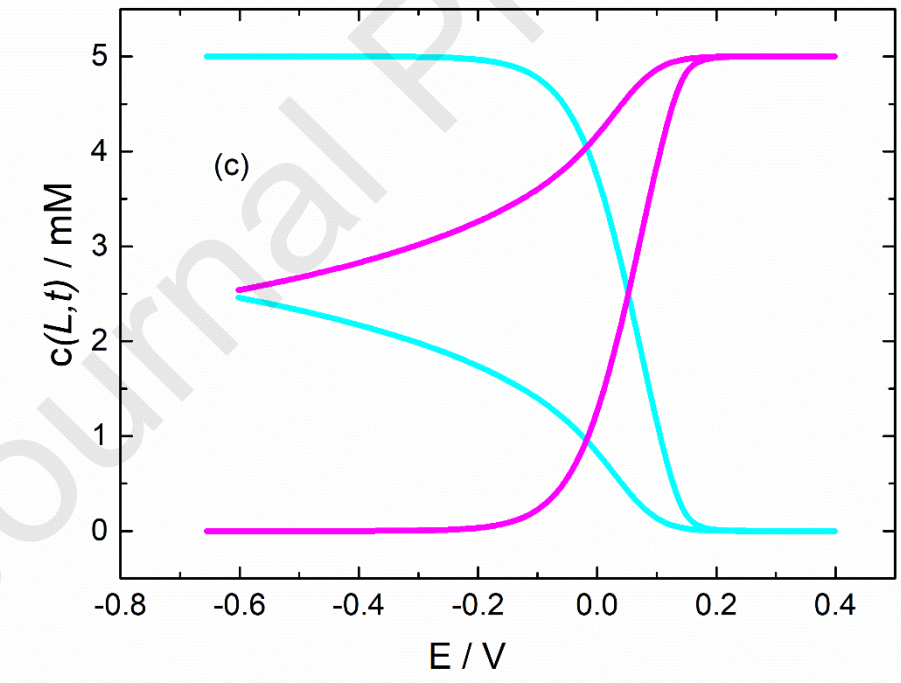

Figure 4

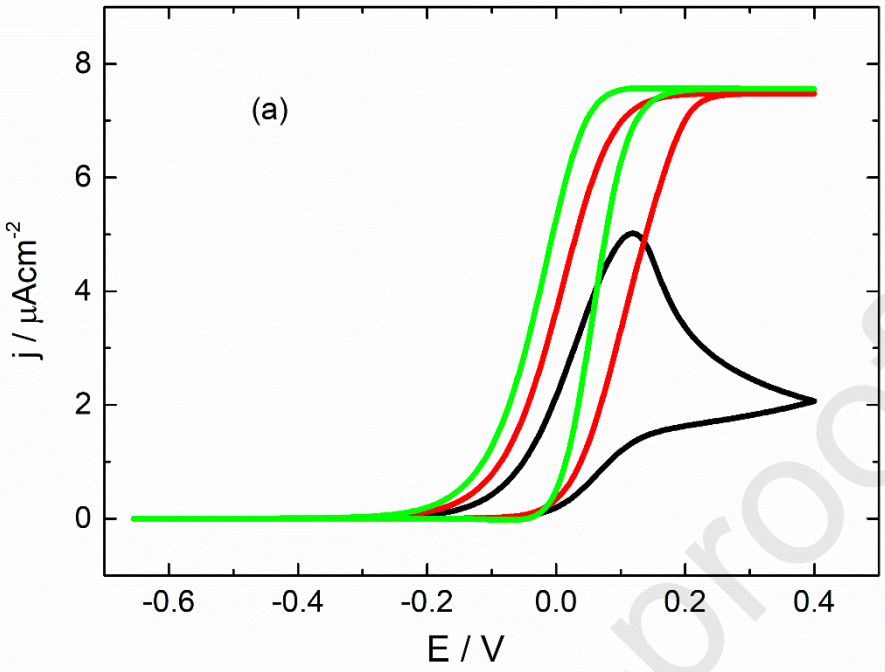

Figure 4

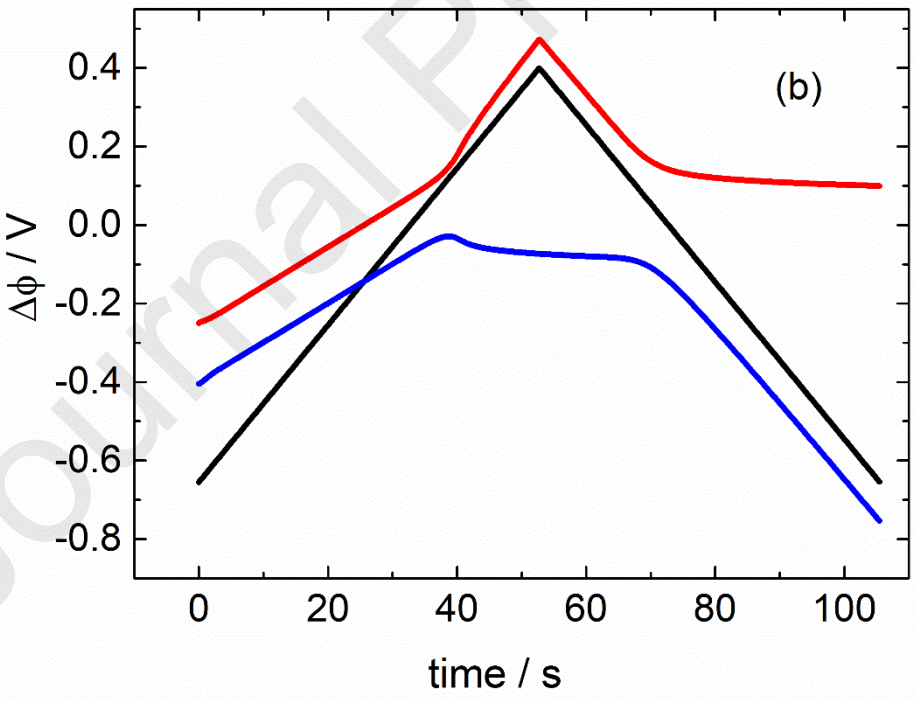

Figure 4

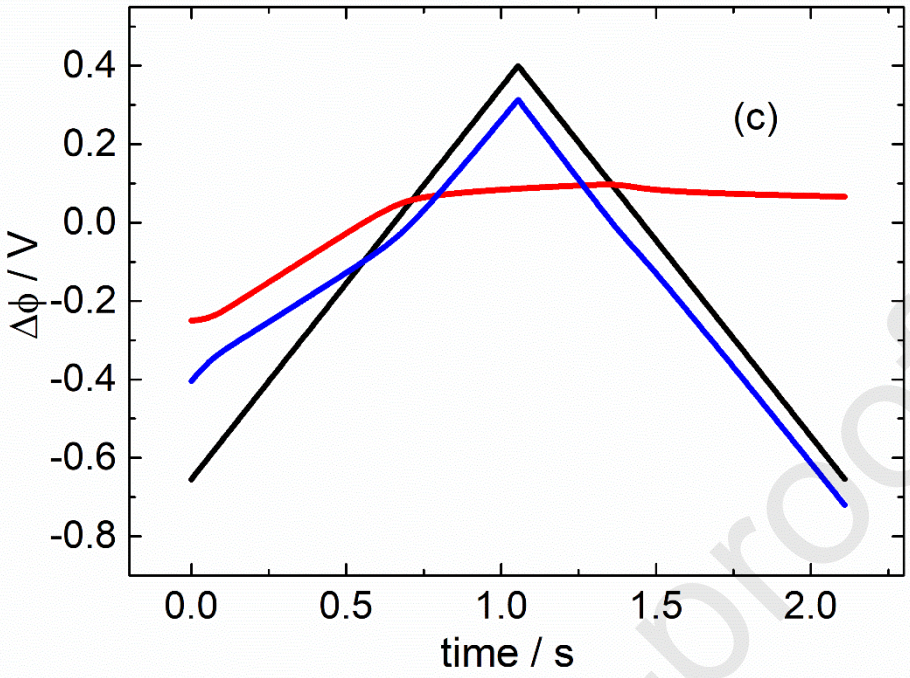

Figure 5

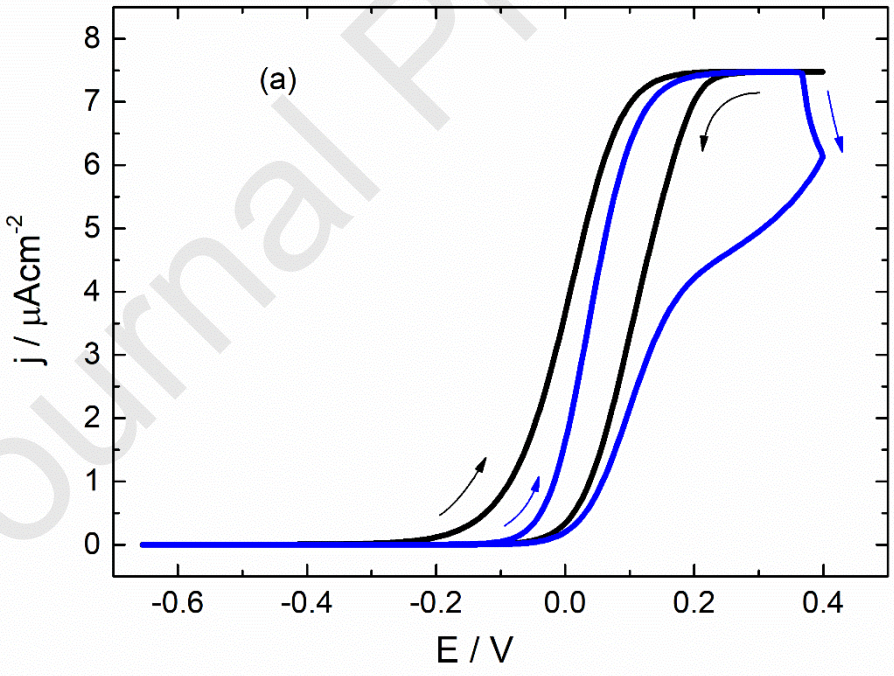

Figure 5

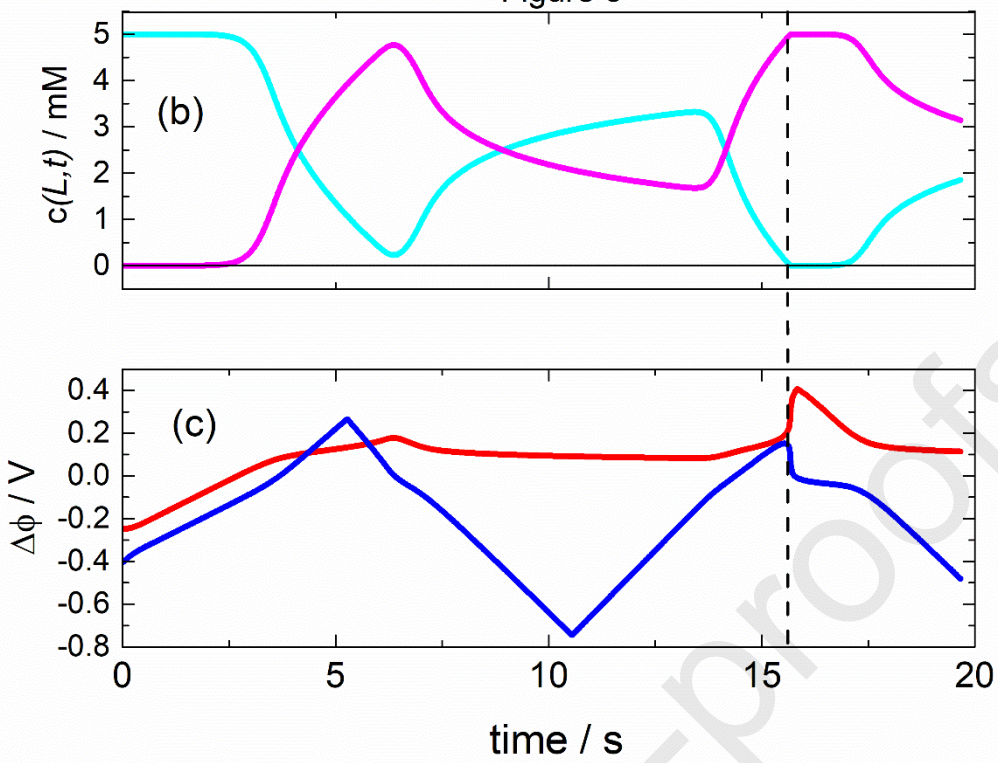

Figure 6

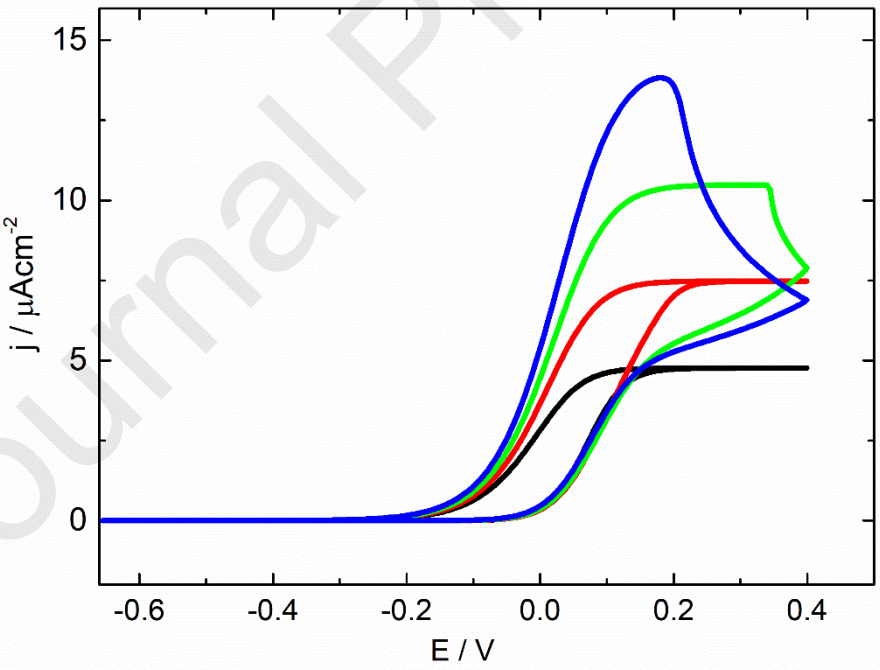

Figure 7

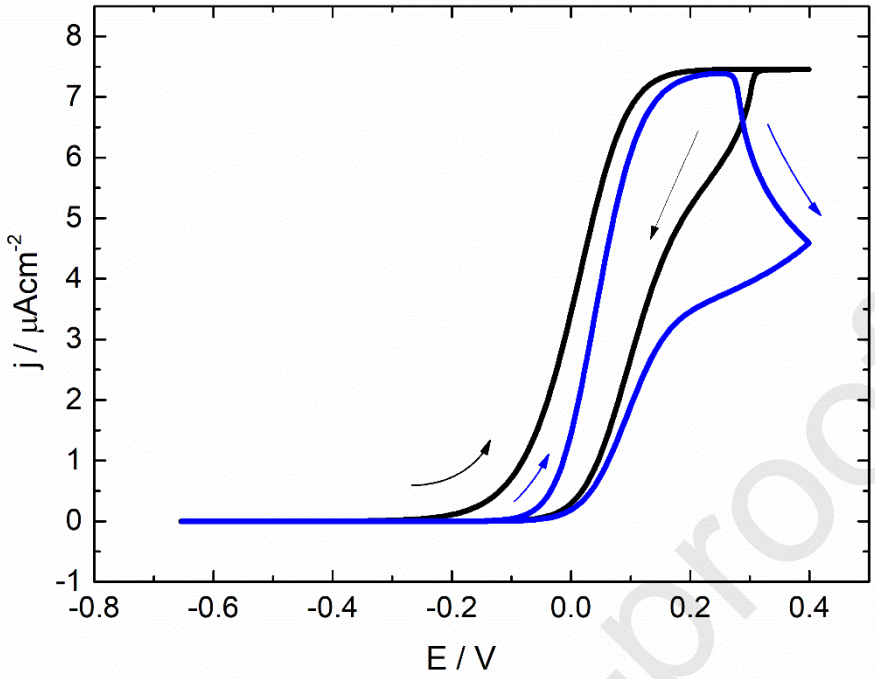

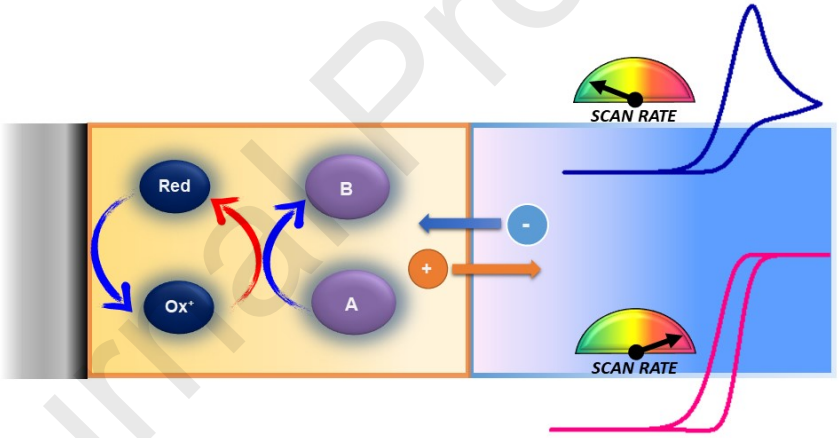

Highlights

>Model including a homogeneous catalytic reaction in a thick-film electrode setup.

>Tunable distribution of the applied potential between the two serial interfaces.

>External parameters allow us to understand how the applied potential is distributed.